JACS
JOURNAL OF THE AMERICAN CHEMICAL SOCIETY

COMMUNICATION

pubs.acs.org/JACS

Ambient Carbon Dioxide Capture by Boron-Rich Boron Nitride Nanotube

Heechol Choi,[†] Young Choon Park,[†] Yong-Hyun Kim,[*,‡] and Yoon Sup Lee[*,†]

[†]Department of Chemistry, Korea Advanced Institute of Science and Technology (KAIST), Daejeon 305-701, Korea
[‡]Graduate School of Nanoscience and Technology (WCU), KAIST, Daejeon 305-701, Korea

Supporting Information

ABSTRACT: Carbon dioxides (CO_2) emitted from large-scale coal-fired power stations or industrial manufacturing plants have to be properly captured to minimize environmental side effects. From results of ab initio calculations using plane waves [PAW-PBE] and localized atomic orbitals [ONIOM(wB97X-D/6-31G*:AM1)], we report strong CO_2 adsorption on boron antisite (B_N) in boron-rich boron nitride nanotube (BNNT). We have identified two adsorption states: (1) A linear CO_2 molecule is physically adsorbed on the B_N, showing electron donation from the CO_2 lone-pair states to the B_N double-acceptor state, and (2) the physisorbed CO_2 undergoes a carboxylate-like structural distortion and C═O π-bond breaking due to electron back-donation from B_N to CO_2. The CO_2 chemisorption energy on B_N is almost independent of tube diameter and, more importantly, higher than the standard free energy of gaseous CO_2 at room temperature. This implies that boron-rich BNNT could capture CO_2 effectively at ambient conditions.

Carbon-based fossil fuels, which presently supply about 80% of the world's energy needs, are the main source of the increasing level of carbon dioxide (CO_2) in the atmosphere. The increased CO_2 level is believed to enhance the greenhouse effect and its global adverse consequences. Sequestration of the CO_2 emitted from coal-fired power stations or industrial manufacturing plants is thus one of the most pressing issues in the environmental protection. An ideal CO_2 sequestration material should have large surface areas and strong adsorption sites that are accessible for *ambient* CO_2 gas. Several CO_2 adsorbents[1−3] have been proposed previously including metal-organic frameworks (MOFs), carbon nanotubes, and silicon carbide (SiC) nanotubes, but the reported CO_2-adsorbent interactions are too weak to be suitable for ambient gas sequestration. Due to their intrinsic high surface areas and polarity, boron nitride nanotube (BNNT) could be a good candidate as CO_2 adsorbent. However, the pristine BNNT with a large band gap is almost inert to the closed-shell CO_2. It is generally expected that the very stable closed-shell molecule will only interact weakly with other materials.

In this communication, on the basis of results of ab initio calculations using theories of plane waves [PAW-PBE][4,5] and localized atomic orbitals [ONIOM(wB97X-D/6-31G*:AM1)],[5,6] we report that a defect site of BNNT can capture CO_2 strongly enough to the ambient-condition sequestration. Among various native defects, we focus on boron antisite (B_N), in which a boron atom sits at the original nitrogen site with being surrounded by three boron atoms, as shown in Figure 1a. The double-acceptor antisite can interact with a CO_2 molecule strongly enough to break a C═O double bond. This type of interaction is analogous with the dihydrogen interaction in boron-doped carbon nanostructures,[7] where a closed-shell H_2 was attracted by a single acceptor state of the carbon-substituted boron.

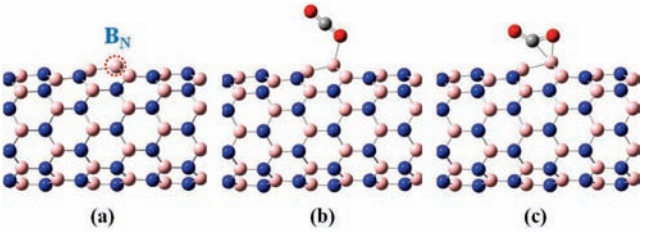

Figure 1. (a) Optimized geometry of boron antisite B_N in (8,0) BNNT. The same of (b) physisorbed and (c) chemisorbed CO_2 on top of the B_N. The B, C, N, and O atoms are represented in pink, gray, blue, and red, respectively.

To search for growth conditions of the defect B_N in BNNT, we calculated defect formation energies (E_{form}) for (8,0) and (10,0) BNNTs in various chemical environments. The defect formation energy is defined as the following:[8]

$$E_{form} = E_{total}[B_N{-}BNNT] - E_{total}[BNNT] + \mu_N - \mu_B \qquad (1)$$

where $E_{total}[B_N{-}BNNT]$ and $E_{total}[BNNT]$ are the PAW-PBE total energies of BNNT with and without the defect, respectively; μ_N and μ_B are the chemical potentials of N and B sources, respectively. For any growth condition of BNNT, it always holds that $\mu_{BN} = \mu_N + \mu_B$. Two limiting growth conditions are thus possible as boron-rich ($\mu_B = \mu_{B,0}$ and $\mu_N = \mu_{BN} - \mu_{B,0}$) and nitrogen-rich ($\mu_N = \mu_{N,0}$ and $\mu_B = \mu_{BN} - \mu_{N,0}$) conditions, where $\mu_{B,0}$ and $\mu_{N,0}$ are the reference systems, respectively. Using eq 1, we calculated formation energies of B_N at various chemical environments, as summarized in Table 1. We could immediately notice that the growth of B_N is much more probable in the boron-rich condition than in the nitrogen-rich limit. The formation energies of B_N vary as well, depending on a type of boron source. When rhombohedral boron (α-B_{12})[9] is used as the boron source, the B_N formation energy is calculated to be 4 eV, which is very comparable to the previous theoretical values.[10] When B_2H_6 gas

Received: November 12, 2010
Published: February 2, 2011

   dx.doi.org/10.1021/ja1101807 | J. Am. Chem. Soc. 2011, 133, 2084–2087

Table 1. Defect Formation Energies (E_{form} in eV) of the Boron Antisite (B_N) in (8,0) and (10,0) BNNTs with Various Chemical Environments, Calculated Using the PAW-PBE Method

	N-rich condition	B-rich condition			
	N_2	α-B_{12}	B_2H_6	B_2H_4	BH_3
(8,0)	8.35	3.99	3.96	1.84	1.76
(10,0)	8.61	4.06	4.03	1.92	1.83

Table 2. Structural Parameters and CO_2 Adsorption Energies (E_{ads}) in (8,0) BNNT with a Boron Antisite (B_N) for the Physisorption and Chemisorption Configurations, Obtained by Using PAW-PBE and ONIOM(wB97X-D/6-31G*:AM1)[a]

	physisorption		chemisorption	
	PAW-PBE	ONIOM	PAW-PBE	ONIOM
$r(B_N-B)$[b]	1.657	1.672	1.817	1.879
$r(B_N-O)$	1.832	1.904	1.600	1.571
$r(B_N-C)$	2.572	2.649	1.732	1.713
$r(C-O)$[c]	1.192	1.178	1.282	1.267
$a(B_N-O-C)$	114.9	116.6	72.9	73.4
$a(O-C-O)$	177.6	178.7	139.0	139.4
E_{ads}	0.21	0.34	0.82	0.74

[a] Bond distance (r) in Å, bond angle (a) in deg, and E_{ads} in eV. [b] The B_N-B bond is parallel to the tube axis as well as the adsorbed CO_2. [c] The C═O bond is located on top of the B_N.

is used, the formation energy is almost the same, 4 eV. However, when the high-energy boron source such as BH_3 or B_2H_4 gas is used, the B_N formation energy is decreased to 1.8−1.9 eV. Therefore, to create many B_N sites in BNNT, one has to keep a boron-rich growth condition and use an energetic boron source such as BH_3 or B_2H_4 gas.

Next, we considered the CO_2 adsorption onto a B_N site of (8,0) BNNT. The structural relaxation with the PAW-PBE method results in the B_N defect protruding outward by about 0.45 Å from the BNNT surface, as shown in Figure 1a. The protruding geometry would facilitate the CO_2 adsorption by reducing steric hindrance from the BNNT side wall.[11]

We identified two distinct adsorptive configurations of CO_2, as shown in b and c of Figure 1 respectively corresponding to physisorption and chemisorption. The CO_2 adsorption energy (E_{ads}) is defined as $E_{ads} = E_{total}(B_N-BNNT) + E_{total}(CO_2) - E_{total}(CO_2 + B_N-BNNT)$. By definition, $E_{ads} > 0$ corresponds to favorable or exothermic adsorption of CO_2 on boron-rich BNNT. The calculated geometrical parameters and adsorption energies of physi- and chemisorbed CO_2 on a B_N are summarized in Table 2. In its physisorbed configuration, the linear CO_2 molecule is slantingly attached to B_N with one O end located almost on top of the defect site, similar to the physisorbed CO_2 on Mg-MOF-74.[2] The B_N-O-C angle is 114.9°, and the B_N-O distance is 1.832 Å, which is much shorter than the van der Waals distance of 3.52 Å. The short B_N-O distance indicates that the CO_2 physisorption is not controlled by typical dispersion forces, but enhanced by some types of chemical interaction. Because of the interaction, the physisorbed CO_2 molecule undergoes small but noticeable structural changes; two C═O bond lengths of the

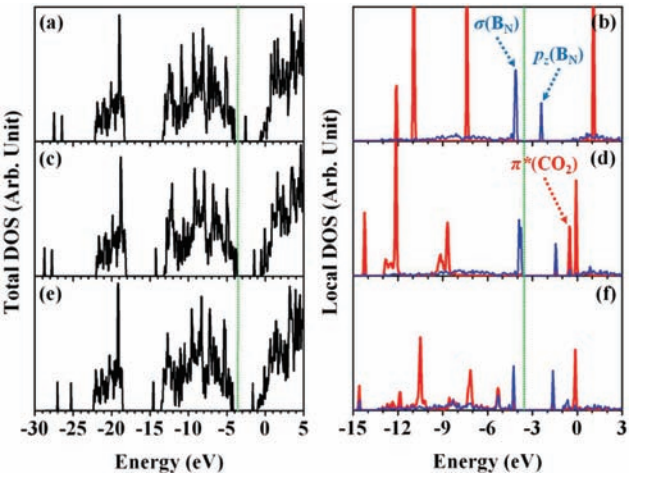

Figure 2. (Left) Total and (right) local density of states (DOS) for (a, b) nonbonding, (c,d) physisorption, and (e,f) chemisorption configurations. The local DOS was projected onto (blue) four boron atoms at the defect site and (red) CO_2. The position of the Fermi level (E_F) is marked by the green line.

physisorbed CO_2 are 1.192 Å and 1.167 Å. The C═O bond close to the B_N site is elongated by 0.015 Å, and the other is shortened by 0.010 Å, compared to 1.177 Å of the free CO_2. The adsorption energy of the physisorbed CO_2 is calculated to be 0.21 eV. In its chemisorbed configuration, the CO_2 molecule undergoes structural distortion to a bent geometry and double-bond breaking of one C═O bond the same way as in forming a carboxylate group. The O−C−O bond angle is 139.0°, and the broken C−O bond is significantly elongated to 1.282 Å on top of the B_N. The defect site is also considerably pulled out by 0.73 Å. The B_N-C and B_N-O distances are 1.732 Å and 1.600 Å, respectively, forming a $C-B_N-O$ triangle similar to the 3-center-2-electron (3c-2e) bonding configuration.[7,12] The triangle is contrasted with the 2 + 2 cycloaddition configuration with a four-membered ring for chemisorbed CO_2 on (8,0) SiC nanotube.[3] The chemisorption energy is calculated to be 0.82 eV in PAW-PBE.

To understand microscopic origins of the enhanced CO_2 physisorption and chemisorption on B_N of BNNT, we performed electronic structure analyses by calculating total and local densities of states (DOS) for nonbonding, physisorption, and chemisorption configurations, as shown in Figure 2a−f. The total DOS clearly shows that the boron-rich BNNT is a large-gap semiconductor with a defect-related gap state. The local DOS plot confirms that the B_N defect introduces the unoccupied double-acceptor defect state in the middle of the energy gap, and also occupied defect states near the valence band edge. Figure 3a−c shows that the occupied defect states have the character of the $pp\sigma$ orbitals, and the unoccupied defect state has the character of the $pp\pi$ or p_z orbital. We named them $\sigma(B_N)$ and $p_z(B_N)$, respectively.

For the nonbonding configuration, in which CO_2 is 8.6 Å away from BNNT, the occupied CO_2 molecular states are distributed at 3−8 eV below the Fermi level (E_F), while the unoccupied $p_z(B_N)$ is at 1.4 eV above E_F. As the CO_2 is physisorbed, the occupied CO_2 states are all down-shifted by up to 2 eV, and the unoccupied $p_z(B_N)$ is up-shifted by 1 eV. This level repulsion corresponds to the so-called electron-donation mechanism because the CO_2 gives its electron to the double-acceptor B_N. For the CO_2 chemisorption configuration, the local DOS plot shows

dx.doi.org/10.1021/ja1101807 |J. Am. Chem. Soc. 2011, 133, 2084–2087

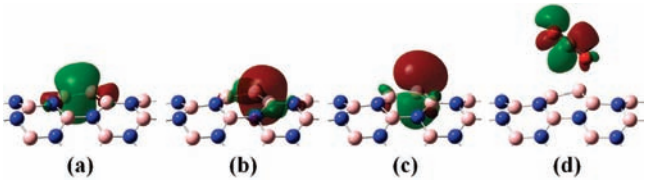

Figure 3. (a,b) Occupied defect states $\sigma(B_N)$ and (c) the unoccupied p_z-like double-acceptor state $p_z(B_N)$ in (8,0) BNNT with a boron antisite. (d) The unoccupied π^*-like CO_2 state of the CO_2-physisorbed configuration, which strongly couples with one of the $\sigma(B_N)$ states in the chemisorption process. The orbital plots are obtained from ONIOM.

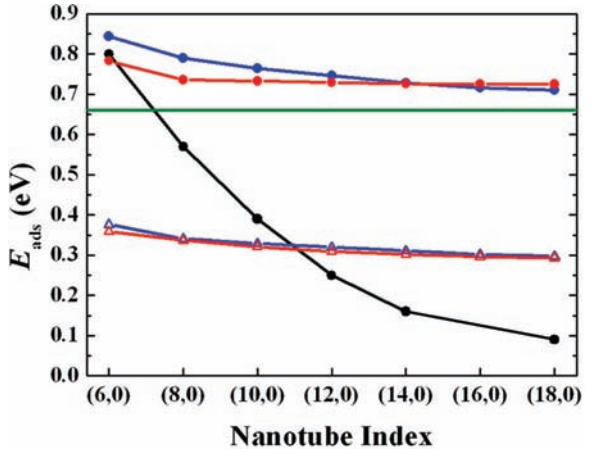

Figure 4. CO_2 adsorption energies on B_N in various (n,0) BNNTs. The red (blue) curve corresponds to the adsorbed CO_2 parallel (oblique) to the tube axis. The solid and open symbols represent chemisorption and physisorption, respectively. The black curve is for CO_2 adsorption energies in (n,0) SiC nanotubes, taken from ref 3 for the sake of contrast. The green line indicates the standard free energy (0.67 eV) of gaseous CO_2 at 300 K. The zero-point energy correction of about 0.04 eV is not included in the plot.

the overall increase of boron states at the valence band due to the level repulsion between one of the occupied $\sigma(B_N)$ states and an unoccupied CO_2 state, $\pi^*(CO_2)$. This level repulsion corresponds to the electron back-donation, namely, electron transfer from BNNT to CO_2. The electron donation−back-donation process leads to the C═O double-bond breaking (1.282 Å from 1.177 Å of the free CO_2) and the B_N−B bond elongation (1.817 Å from 1.636 Å in the nonbonding configuration).

The ONIOM method produces more or less the same CO_2 adsorption characteristics, as compared with that from PAW-PBE (Table 2). The difference between two methods is within about 0.08 Å for bond length and about 2° for bond angle. Such a remarkable agreement can be attributed to the localized character of the CO_2−B_N interaction. The dispersion-corrected physisorption energy of 0.34 eV using the wB97X-D functional is comparable to 0.43 eV for the physisorbed CO_2 in Mg-MOF-72.[2] Note that in ref 2 theory and experiment agree very well. From natural population analysis,[5] we confirmed that 0.19 electron is indeed donated from the CO_2 molecule to the defect site in the physisorption configuration, whereas 0.26 electron is back-donated in the chemisorption configuration. By performing IRC calculations,[5] we could identify a transition state (TS) between the physisorption and chemisorption configurations. Thus, the chemisorption process has the small reaction energy barrier of 0.043 eV from the physisorption configuration. The physisorption process has no TS.

By using the efficient hybrid approach of ONIOM, we could extensively investigate CO_2 adsorption characteristics on B_N for various configurations and BNNTs. We found that CO_2 physi- and chemisorption energies on the defect site are almost independent of BNNT diameters and bonding directions. As displayed in Figure 4, almost constant adsorption energies of CO_2 are obtained for various (n,0) BNNTs, where n = 6, 8, 10, 12, 14, 16, and 18. The red (blue) curve in Figure 4 is for the adsorbed CO_2 parallel (oblique) to tube axis. This is again attributed to the localized character of the CO_2−B_N interaction.

Of special interest is that the chemisorption energies are all greater than the standard free energy of gaseous CO_2, i.e., 0.67 eV at 300 K. This is clearly an advantage of boron-rich BNNT over the previously proposed adsorbents,[1,2] namely, capturing CO_2 at ambient conditions. Also, boron-rich BNNT has an additional merit over SiC nanotubes, for the CO_2 interaction strength on SiC nanotubes is strongly diameter dependent,[3] as shown in Figure 4.

In conclusion, ab initio calculation results suggest that the boron antisite (B_N) defect of boron-rich BNNT could capture CO_2 at ambient conditions. The CO_2 capture would be initiated with a barrier-less physisorption process due to the electron donation from CO_2 to the double-acceptor defect site, and proceed to the chemisorption state by breaking one C═O double bond. Finally, we are actively investigating the potential of utilizing the CO_2-adhesive B_N defect as a catalyst for the CO_2 conversion to fuel, for example, to formic acid (HCOOH).

■ ASSOCIATED CONTENT

Ⓢ Supporting Information. Computational details of PAW-PBE and ONIOM(wB97X-D/6-31G*:AM1). Optimized geometric parameters and relative energies of stationary points on the CO_2 adsorption paths. This material is available free of charge via the Internet at http://pubs.acs.org.

■ AUTHOR INFORMATION

Corresponding Author
yong.hyun.kim@kaist.ac.kr; yslee@kaist.edu

■ ACKNOWLEDGMENT

This work was supported by the National Research Foundation of Korea (NRFK) Grants (NRF-2009-351-C00123, 2009-0076263, and 2010-0001632) and the EEWS program of KAIST. Y.H.K was supported by the WCU program (R31-2008-000-10071-0) and Basic Science Research program (2010-0006922) through the NRFK.

■ REFERENCES

(1) (a) Pulido, A.; Delgado, M. R.; Bludský, O.; Rubeš, M.; Nachtigall, P.; Areán, C. O. *Energy Environ. Sci.* **2009**, *2*, 1187. (b) Gray, M. L.; Soong, Y.; Champagne, K. J.; Pennline, H.; Baltrus, J. P., Jr.; Khatri, R.; Chuang, S. S. C.; Filburn, T. *Fuel Process. Technol.* **2005**, *86*, 1449. (c) Banerjee, R.; Phan, A.; Wang, B.; Knobler, C.; Furukawa, H.; O'Keeffe, M.; Yaghi, O. M. *Science* **2008**, *319*, 939. (d) Zhao, J.; Buldum, A.; Han, J.; Lu, J. P. *Nanotechnology* **2002**, *13*, 195. (e) Bienfait, M.; Zeppenfeld, P.; Dupont-Pavlovsky, N.; Muris, M.; Johnson, M. R.; Wilson, T.; DePies, M.; Vilches, O. E. *Phys. Rev. B* **2004**, *70*, 035410. (f) Matranga, C.; Bockrath, B. *J. Phys. Chem. B* **2005**, *109*, 9209. (g) Lu, C.; Bai, H.; Wu, B.; Su, F.; Hwang, J. F. *Energy Fuels* **2008**, *22*, 3050.

(2) Valenzano, L.; Civalleri, B.; Chavan, S.; Palomino, G. T.; Areán, C. O.; Bordiga, S. *J. Phys. Chem. C* **2010**, *114*, 11185.
(3) Zhao, J. X.; Ding, Y. H. *J. Chem. Theory Comput.* **2009**, *5*, 1099.
(4) (a) Kresse, G.; Joubert, D. *Phys. Rev. B* **1999**, *59*, 1758. (b) Perdew, J. P.; Burke, K.; Ernzerhof, M. *Phys. Rev. Lett.* **1996**, *77*, 3865.
(5) See the Supporting Information.
(6) (a) Maseras, F.; Morokuma, K. *J. Comput. Chem.* **1995**, *16*, 1170. (b) Chai, J.; Head-Gorden, M. *Phys. Chem. Chem. Phys.* **2008**, *10*, 6615. (c) Hariharan, P. C.; Pople, J. A. *Theor. Chim. Acta* **1973**, *28*, 213. (d) Dewar, M. J. S.; Zoebisch, E. G.; Healy, E. F.; Stewart, J. J. P. *J. Am. Chem. Soc.* **1985**, *107*, 3902.
(7) Kim, Y.-H.; Zhao, Y.; Williamson, A.; Heben, M. J.; Zhang, S. B. *Phys. Rev. Lett.* **2006**, *96*, 016102.
(8) Zhang, S. B.; Northrup, J. E. *Phys. Rev. Lett.* **1991**, *67*, 2339.
(9) Oganov, A. R.; Chen, J.; Gatti, C.; Ma, Y.; Ma, Y.; Glass, C. W.; Liu, Z.; Yu, T.; Kurakevych, O. O.; Solozhenko, V. L. *Nature* **2009**, *457*, 863.
(10) (a) Schmidt, T. M.; Baierle, R. J.; Piquini, P.; Fazzio, A. *Phys. Rev. B* **2003**, *67*, 113407. (b) Wu, X.; Yang, J.; Hou, J. G.; Zhu, Q. *J. Chem. Phys.* **2006**, *124*, 054706.
(11) Li, X. M.; Tian, W. Q.; Huang, X. R.; Sun, C. C.; Jiang, L. *J. Nanopart. Res.* **2009**, *11*, 395.
(12) Rasul, G.; Prakash, G. K. S.; Olah, G. A. *J. Am. Chem. Soc.* **1999**, *121*, 7401.